IET Power Electronics

Research Article

IET Journals
The Institution of Engineering and Technology

Non-linear adaptive hysteresis band pulse-width modulation control for hybrid active power filters to reduce switching loss

ISSN 1755-4535
Received on 4th November 2014
Revised on 31st March 2015
Accepted on 9th May 2015
doi: 10.1049/iet-pel.2014.0824
www.ietdl.org

Lei Wang[1] ✉, *Chi-Seng Lam*[1,2], *Man-Chung Wong*[1,2], *Ning-Yi Dai*[1], *Keng-Weng Lao*[1], *Chi-Kong Wong*[1]

[1]*Department of Electrical and Computer Engineering, Faculty of Science and Technology, University of Macau, Macao, People's Republic of China*
[2]*State Key Laboratory of Analog and Mixed-Signal VLSI, University of Macau, Macao, People's Republic of China*
✉ *E-mail: jordanwanglei@gmail.com*

Abstract: Pulse-width modulations (PWMs) are widely investigated in active power filter (APF) applications. However, there are seldom PWMs proposed in hybrid APF (HAPF) applications because of their non-linear current characteristic. This study proposes a non-linear adaptive hysteresis band PWM controller for HAPFs to reduce the switching loss and keep the total harmonic distortion (THD) at an acceptable level. In contrast to previous studies, as the coupling LC impendence of an HAPF can yield a non-linear compensating current, the quasi-linear and non-linear regions are exploited to obtain a low switching frequency. In addition, an approximated THD index is proposed to assess THD in a simplified way in the control system, which results in a faster system response. Finally, the performance of the non-linear adaptive hysteresis band controller is verified by comparing simulation and experimental results with a state-of-the-art PWM for HAPFs.

1 Introduction

Since the first installation of passive power filters (PPFs) in the mid-1940s, PPFs have been widely used to suppress harmonic currents and compensate reactive power. Unfortunately, they suffer many disadvantages such as low dynamic performance, resonance problems and sensitivity to system parameter variation [1–4]. Active power filters (APFs) can address the inherent problems in PPFs, but their initial and operational costs are relatively high.

Different pulse-width modulations (PWMs), from hysteresis to space-vector modulations (SVMs), have been proposed for controlling APFs [5]. For example, PWM methods such as ramp comparison, ripple prediction [6, 7] and improved asymmetric SVM [8] were developed to obtain faster dynamics and greater robustness. Wei and Lukaszewski [9] investigated an algorithm that doubles the switching frequency in the area where the ripple current is larger. This algorithm could reduce switching loss under the same current ripple requirements. However, all of the above PWMs are dedicated for APFs.

Srianthumrong and Akagi [1] proposed an LC-coupled hybrid APF (HAPF) with a low dc-link voltage to reduce the cost of APFs. To date, two main strategies have been used to control HAPFs:

- Equivalent resistor transfer function [1, 3, 10–13].
- Hysteresis PWM [4, 14–19].

The equivalent resistor transfer function can be classified as an indirect current control (multiplying the reference current by a gain) to calculate the voltage reference, which is then inserted back into the equivalent circuit as a system transfer function to characterise the total system response. In contrast, the hysteresis band defines the allowable error in the current that turns the power electronic switches on or off. The non-linear current characteristics of the hysteresis PWM approach were not studied by in 2009 [2]. Until 2012, the non-linear current characteristics were studied and classified into non-linear, quasi-linear and linear regions in [17]. In [17], the non-linear current was linearised under the criteria defined in [17] for power electronic switching so that HAPFs could be equivalent to linear systems, such as active filter operations. On the basis of [18], the minimum dc-link voltage could be defined and calculated. Finally, adaptive dc-link voltage-controlled HAPFs could be implemented in [14, 18, 19]. However, the state-of-the-art hysteresis PWM approach still suffers from relatively high switching loss.

In this paper, considering the users' requirements of total harmonic distortion (THD), a non-linear adaptive hysteresis band controller for HAPFs is proposed. The advantages of the proposed method are:

- *A fast performance index:* An approximated THD (ATHD) is proposed for HAPFs to instantaneously assess the THD value. The ATHD can be controlled to track the reference ATHD* instantaneously according to users' requirements.
- Compared with the state-of-the-art hysteresis PWM control methods [14, 17–19], this paper proposes that the compensating current of HAPFs can operate in non-linear or quasi-linear regions in some circumstances to reduce the switching loss, instead of always staying in a linear region.
- On the basis of the deduced ATHD and non-linear characteristics of HAPFs, a non-linear adaptive hysteresis band PWM controller for HAPFs is proposed to reduce the switching loss and keep the THD at an acceptable level.

In this paper, the circuit configuration of an HAPF is given in Section 2. Its corresponding mathematical model and non-linear current characteristics are introduced in Section 3. In Section 4, the suggested ATHDs are discussed and the non-linear adaptive hysteresis band control for HAPFs is addressed. In Section 5, the simulated and experimental results are reported to verify the proposed approach. Moreover, comparisons with other recently developed methods are also provided. Finally, a conclusion is presented in the last section.

2 Circuit configuration of a three-phase four-wire centre-split HAPF

The circuit configuration of the three-phase four-wire centre-split HAPF is shown in Fig. 1. In the below analysis, the subscript '*x*'

© The Institution of Engineering and Technology 2015

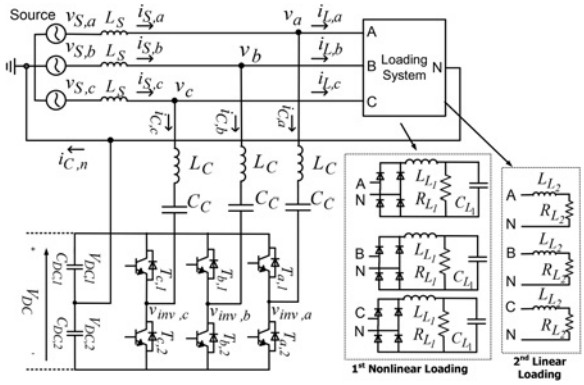

Fig. 1 *Circuit configuration of a three-phase four-wire centre-split power filter*

denotes phases $x = a$, b, c and n; $v_{S,x}$ is the system voltage; v_x is the terminal load voltage; L_S is the system inductor; L_C is the coupling inductor; C_C is the coupling capacitor; $i_{S,x}$, $i_{L,x}$ and $i_{C,x}$ are the source, load and compensating currents, respectively; $v_{inv,x}$ is the inverter voltage; $C_{DC,1}$ and $C_{DC,2}$ are the upper and lower dc-link capacitors, respectively; $V_{DC,1}$ and $V_{DC,2}$ are the upper and lower dc-link voltages, respectively; and V_{DC} is the total dc-link voltage. To verify the transient performance of the proposed control method, two loads are building for testing. One is an RL linear load and the other is a full bridge rectifier non-linear load.

In this configuration, as the coupling LC can yield a non-linear compensating current slope, the non-linear characteristics of the HAPF compensating current $i_{C,x}$ will be discussed in the following section.

3 Compensating current characteristics of HAPF

From Fig. 1, a mathematical model for an HAPF can be deduced. The relationships among the compensating current $i_{C,x}$, coupling inductor L_C, coupling capacitor C_C and inverter voltage $v_{inv,x}(t)$ of an HAPF are calculated as

$$L_C \frac{di_{C,x}(t)}{dt} + \frac{1}{C_C}\int i_{C,x}(t)\,dt = v_x(t) - v_{inv,x}(t) \tag{1}$$

Taking the derivative of (1) yields

$$L_C \frac{d^2 i_{C,x}(t)}{dt^2} + \frac{1}{C_C} i_{C,x}(t) = \frac{d[v_x(t) - v_{inv,x}(t)]}{dt} \tag{2}$$

It can be clearly observed that (2) is a second-order equation in terms of $i_{C,x}(t)$. The time-domain solution of $i_{C,x}(t)$ is deduced below to show its characteristics.

Take the Laplace transform of (2) and simplify it. Next, substitute the initial compensating current and capacitor voltage conditions into the characteristic Laplace equation. Finally, the time-domain solution $i_{C,x}(t)$ can be obtained by taking the inverse Laplace transformation

$$i_{C,x}(t) = A \cdot \sin(\omega_0 t + \phi) \tag{3}$$

where

$$A = \sqrt{i_{C,x}^2(0) + \frac{C_C}{L_C} \cdot [v_x(t) - v_{inv,x}(t) - v_{C_C}(0)]^2}$$

$$\omega_0 = \frac{1}{\sqrt{L_C \cdot C_C}}$$

and

$$\phi = \tan^{-1}\left(\frac{\sqrt{L_C}}{\sqrt{C_C}} \cdot \frac{i_{C,x}(0)}{v_x(t) - v_{inv,x}(t) - v_{C_C}(0)}\right)$$

The compensating current $i_{C,x}(t)$ is expressed in terms of the coupling inductor L_C, coupling capacitor C_C, initial compensating current $i_{C,x}(0)$, initial capacitor voltage $v_{C_C}(0)$, load voltage $v_x(t)$ and inverter voltage $v_{inv,x}(t)$. The value of $v_{inv,x}(t)$ can be obtained from the dc-link voltage V_{DC} and switching states.

As the coupling part of an HAPF is an LC circuit, the mathematical model in terms of $i_{c,x}(t)$ is the second-order differential equation as (2) and the compensating current $i_{c,x}(t)$ solution in the time domain contains a sine function, as shown in (3). Equation (3) aims to show the non-linear characteristics and transient response of the compensating current in an HAPF during each switching (on or off) interval. The value of ω_0 in (3) depends on the coupling components only, rather than the system frequency ($\omega_f = 2\pi f$). Moreover, its amplitude A varies because of the different initial conditions at each moment. On the basis of the relationship between the hysteresis band H and amplitude A, three operating regions for the HAPF compensating current can be defined: the linear, quasi-linear and non-linear regions, as shown in Fig. 2.

In the linear region shown in Fig. 2*a*, the slope of the compensating current can be treated as linear if the hysteresis band is set small enough ($H \ll A$). In the linear region, the switching time t_{sw} is relatively small, which is the key to linearising the current slope, as discussed in [17].

In the quasi-linear region (Fig. 2*b*), the slope polarity of the compensating current interchanges once $i_{C,x}$ touches the top or bottom hysteresis band with $H \simeq A$. Under this region, the switching time t_{sw} increases compared with the linear region case. Therefore the switching frequency f_{sw} and power loss P_{loss} decrease.

As shown in Fig. 2*c*, the non-linear region case can occur when the hysteresis band is set to be larger than the amplitude ($H > A$). In the non-linear region, the compensating slope polarity interchanges before $i_{C,x}$ touches the top or bottom hysteresis band. A large H value would enlarge the output current ripple and degrade the system performance. However, this region does not generate trigger signals to the switching devices; thus, f_{sw} and P_{loss} can be minimised.

It is interesting to further investigate the quasi-linear and non-linear regions. In these two operation modes, less f_{sw} is required, but the current tracking error is still within the set hysteresis band. Therefore the reduction of the switching frequency can be achieved by enlarging the hysteresis band. However, when the hysteresis band is too large, the THD is poor and the system performance deteriorates. Thus, it is essential to investigate the conditions such that the HAPF compensation performance is within requirements, with a reduction in the switching frequency to reduce unnecessary loss.

As the amplitude of the compensating current A varies because of different initial conditions at different switching intervals, the compensating current may operate in three different regions. A simulation for the probability of the compensating current falling in different regions is performed based on the system parameters defined in Section 5 and is summarised in Fig. 3.

In Fig. 3, the probabilities of an HAPF operating in the linear, quasi-linear and non-linear regions are calculated by dividing the time duration in these regions (t_{linear}, t_{quasi} and $t_{non\text{-}linear}$) by the fundamental period t_f. The curves of t_{linear}/t_f and $(t_{non\text{-}linear} + t_{quasi})/t_f$ are obtained by taking their average values over the entire simulated periods. The time duration in the linear region t_{linear} is the sum of all the switching time periods t_{sw} within the linear region over one fundamental period. If the HAPF is not operating in a linear region, then it is operating in a non-linear or quasi-linear region.

Referring to Fig. 2, if the hysteresis band H is set to be small, the switching frequency is higher and the THD becomes lower; thus, the possibility of the HAPF compensating current falling in the linear

© The Institution of Engineering and Technology 2015

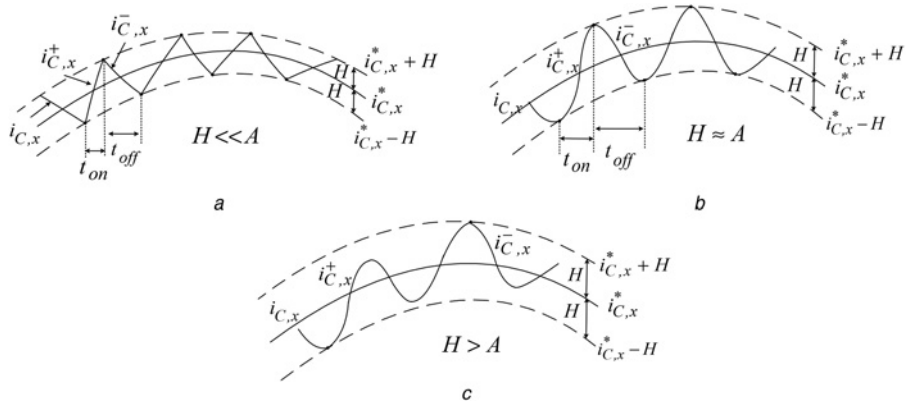

Fig. 2 *Different operating regions for HAPF compensating current based on the relationship between the hysteresis band H and amplitude A*

a Linear region
b Quasi-linear region
c Non-linear region

region becomes higher, and vice versa. To reduce the HAPF switching power loss P_{loss}, the time duration for operating in the non-linear or quasi-linear regions $(t_{\text{non-linear}} + t_{\text{quasi}})/t_{\text{f}}$ can be increased, whereas that for the linear region $t_{\text{linear}}/t_{\text{f}}$ can be decreased.

With reference to the IEEE Standards 519-2014 [20], the total demand distortion (TDD) = 15% and $I_{\text{SC}}/I_{\text{L}}$ is typically in 100 < 1000 scale. The nominal rate current is assumed to be equal to the fundamental load current in the worst case, which results in THD = TDD = 15%. Therefore this paper focuses on a THD below 15%.

In the following section, a non-linear adaptive hysteresis band PWM controller for HAPFs is proposed, in which a balance between the low THD in the linear region and the low switching loss in the non-linear region is achieved.

4 Non-linear adaptive hysteresis band PWM controller for HAPFs

In this section, the proposed non-linear adaptive hysteresis band PWM controller is discussed. First, the relationship between hysteresis bands and ATHD is addressed. Second, the control block diagram of the proposed non-linear adaptive hysteresis band PWM controller for HAPFs is illustrated.

4.1 Relationship between hysteresis band H and ATHD

The relationship between a hysteresis band H and the harmonic distortion in a source current is deduced in this section. The HAPFs inject compensating current to the point of common coupling. If the compensating current is exactly the same as its reference, the source current $i_{\text{S},x}$ will be a sinusoidal wave without distortion. However, the difference between the reference current and the compensating current varies in terms of the hysteresis band H, as discussed in Section 3. As a result, the compensating current waveform can be approximately decomposed into a reference compensating current $i^*_{\text{C},x}$ and current tracking error. The waveform of current tracking error is either an irregular triangle waveform (linear region) or a sinusoidal-like (non-linear region) waveform, as shown in Fig. 4.

The root-mean-square (RMS) value of the current error I_{e} can be estimated by

$$I_{\text{e}} = \sqrt{\frac{1}{t_{\text{f}}}\left(\int_0^{t_1} i_{\text{e}}^2\,\text{d}t + \int_{t_1}^{t_2} i_{\text{e}}^2\,\text{d}t + \cdots + \int_{t_{n-1}}^{T_{\text{f}}} i_{\text{e}}^2\,\text{d}t\right)} \simeq \frac{H}{k} \quad (4)$$

where t_{f} is the fundamental period and k is a factor with a range of $k \in [\sqrt{2}, \sqrt{3}]$. The value of k is $\sqrt{3}$ when the compensating current is fully in the linear region. Its value is $\sqrt{2}$ when the compensating current is fully in the non-linear region. The detailed calculation of the k value under these two situations is provided in Appendix. When the compensating current falls in both linear region and non-linear region during HAPFs operation, the value of k is calculated as the sum of the product of the probabilities and corresponding factors

$$k = \sqrt{3} \cdot \frac{t_{\text{linear}}}{t_{\text{f}}} + \sqrt{2} \cdot \frac{(t_{\text{non-linear}} + t_{\text{quasi}})}{t_{\text{f}}} \quad (5)$$

where the probabilities can be obtained from Fig. 3. Hence, the value of k is a pre-defined constant and can be used to calculate RMS value of the current tracking errors when the target THD* of the source current is set.

Generally, the harmonic distortion of the source current after compensation is assessed by THD, which is defined as the ratio between the RMS values of the harmonic and fundamental components [21]

$$\text{THD} = \frac{\sqrt{\sum_{n=2}^{\infty} I_n^2}}{I_1} \times 100\% = \frac{I_{\text{h}}}{I_1} \times 100\% \quad (6)$$

where I_1 is the fundamental current and I_{h} is the RMS value of harmonic currents. During HAPF operation, the fundamental source current $I_{\text{S},1}$ consists of only active power component, whereas the reactive power component is compensated by the

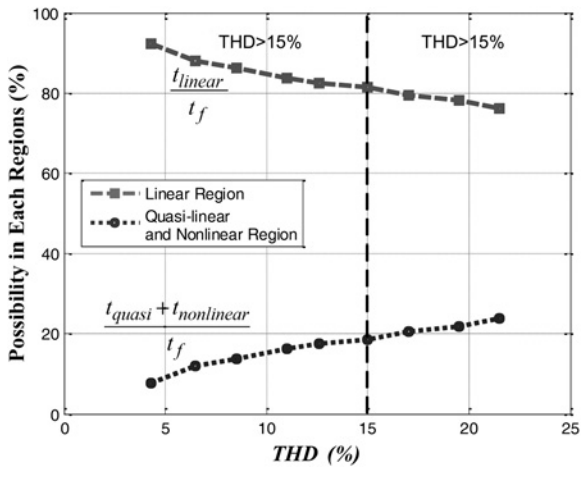

Fig. 3 *Relationship between the operation probability in each region and THD*

IET Power Electron., 2015, Vol. 8, Iss. 11, pp. 2156–2167
© The Institution of Engineering and Technology 2015

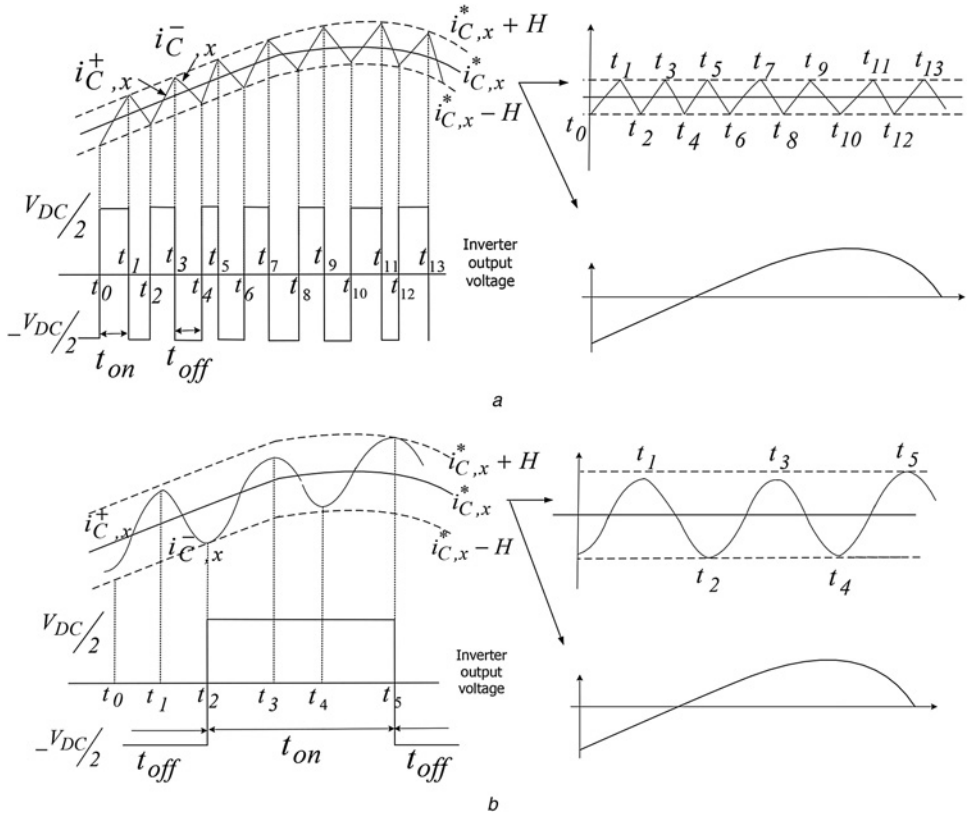

Fig. 4 *Proposed current THD analysis method*

a Linear region
b Non-linear region

HAPF. Therefore the fundamental source current value $I_{S,1}$ can be calculated as

$$I_{S,1} = \frac{\bar{p}_{\alpha\beta}}{\sqrt{3} \cdot \|v_L\|} \tag{7}$$

where

$$\|v_L\| = \sqrt{v_a^2 + v_b^2 + v_c^2} \tag{8}$$

in which $\|v_L\|$ is the norm or magnitude of the load voltage. $\bar{p}_{\alpha\beta}$ can be obtained by passing the loading instantaneous active power $p_{\alpha\beta}$ through a low-pass filter [22].

To obtain I_h via fast Fourier transform is complex and time-consuming. By using the RMS value of current tracking error $I_e$in (4) to replace I_h in (6), an ATHD value is proposed in this paper, which is expressed as

$$\text{ATHD} = \frac{I_e}{I_{S,1}} \times 100\% = \frac{H}{k \cdot I_{S,1}} \times 100\% \tag{9}$$

Table 1 HAPF simulated and experimental system parameters for power quality compensation

	Parameters	Physical values
system parameters	v_x, f and L_S	110 V, 50 Hz and 1 mH
HAPF parameters	L_C and C_C	5 mH and 80 μF
	$C_{DC,1}$ and $C_{DC,2}$	5 and 5 mF
	$V_{DC,1}$ and $V_{DC,2}$	50 and 50 V
first non-linear loading	L_{L1}, R_{L1} and C_{L1}	30 mH, 32 Ω and 400 μF
second linear loading	L_{L2} and R_{L2}	80 mH and 50 Ω

In contrast to (4), a constant coefficient k and the adaptive hysteresis band H are used to assess current distortion. The calculation is greatly simplified.

The ATHD is proposed to simplify the calculation steps and to speed up the determination of the system performance in real time. By using H in ATHD, the computation can avoid the time consumption required for actual current error calculations. However, the ATHD is an estimated THD index rather than the real THD. On the basis of the system parameters given in Table 1, a comparison between the THD and ATHD values is provided in Fig. 5. Both THD and ATHD increase as H increases. It can be concluded from Fig. 5 that the difference between THD and ATHD is small at THD < 15%. Thus, it is acceptable to use ATHD in place of THD if the source current distortion is kept below 15%.

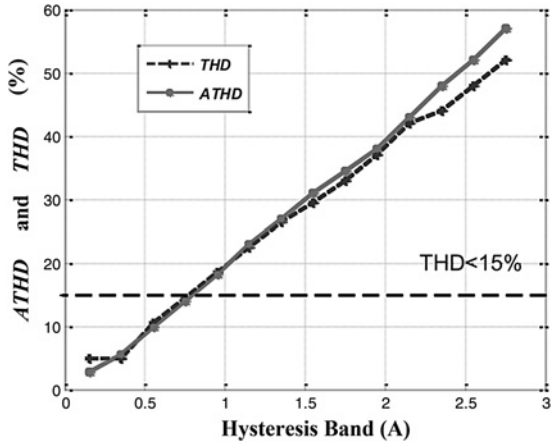

Fig. 5 *Comparison of THD and ATHD*

© The Institution of Engineering and Technology 2015

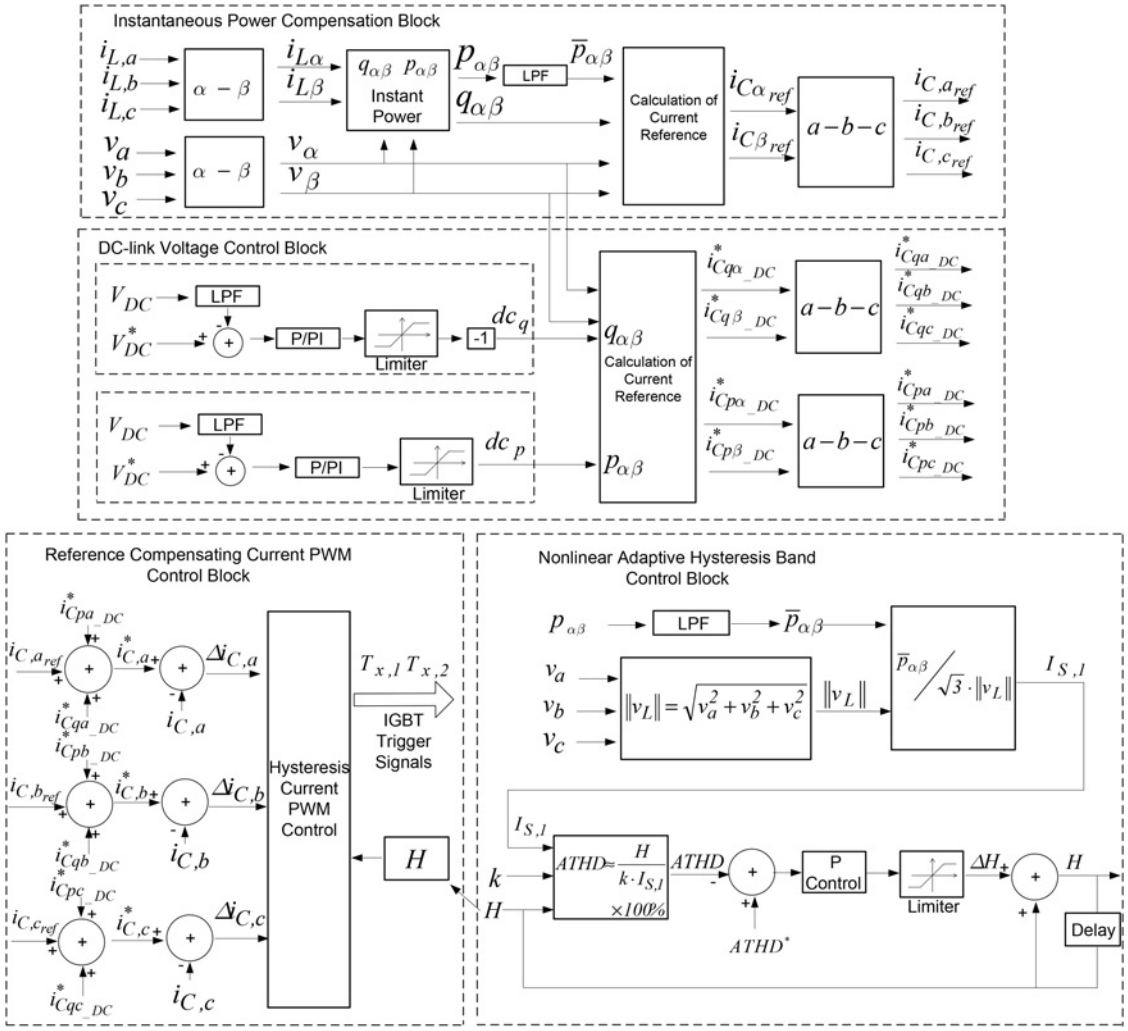

Fig. 6 *Control block diagram of the proposed non-linear adaptive hysteresis band PWM control for HAPFs*

Figs. 3 and 5 are used to explain the relationship among different HAPF operation regions, H and THD values:

- When H is set to be small, the THD value is improved. Moreover, the possibility of the HAPF operating in the linear region is higher and that in the non-linear region is lower, thus leading to a higher switching frequency (power loss).
- When H is set to be large, the THD value becomes worst. The possibility of the HAPF operating in the non-linear region is increasing and that in the linear region is decreasing, thus leading to a lower switching frequency (power loss).
- To achieve a balance between the power loss and system performance, a higher reference THD* can be set according to the users' design requirement (satisfying IEEE Standards 519–2014). Therefore even the THD compensation performance by the HAPF may not be as good as it is designed to be when operating within the linear region [17]. When the system is operated in the non-linear region, the switching loss can be significantly reduced.

In the following section, a control block diagram of the proposed non-linear adaptive hysteresis band PWM controller is given based on the above discussion.

4.2 Control block diagram of the proposed non-linear adaptive hysteresis band controller for HAPF

On the basis of the above discussion, a control block diagram of the proposed non-linear adaptive hysteresis PWM band controller for HAPFs is shown in Fig. 6. The overall controller for HAPFs consists of four parts: (i) the instantaneous power compensation control, (ii) the dc-link voltage control, (iii) the reference compensating current PWM control and (iv) the non-linear adaptive hysteresis band control. A detailed discussion of the instantaneous power compensation control and reference compensating current PWM control is provided in [22].

For the dc-link voltage control shown in Fig. 6, the HAPF can effectively control the dc-link voltage by feeding back the dc voltage-controlled signals dc_q and dc_p [18, 19]

$$\mathrm{dc}_q = -k_q \cdot (V_{\mathrm{dc}}^* - V_{\mathrm{dc}}) \tag{10}$$

$$\mathrm{dc}_p = k_p \cdot (V_{\mathrm{dc}}^* - V_{\mathrm{dc}}) \tag{11}$$

where k_q and k_p are the proportional gains of the dc-link voltage controller; dc_q and dc_p are the dc control signals related to the reactive and active current components, respectively; dc_q aims to step change the dc-link voltage under insufficient dc-link voltage during the start-up process; and dc_p aims to maintain the dc-link voltage [18].

The hysteresis PWM control method (current reference) is applied. Therefore dc_q and dc_p are transferred to the current references in a–b–c coordinates based on the three-phase instantaneous pq theory [22] shown by the equations below

IET Power Electron., 2015, Vol. 8, Iss. 11, pp. 2156–2167
© The Institution of Engineering and Technology 2015

$$\begin{bmatrix} i^*_{\mathrm{C},ap\_\mathrm{DC}} \\ i^*_{\mathrm{C},bp\_\mathrm{DC}} \\ i^*_{\mathrm{C},cp\_\mathrm{DC}} \end{bmatrix} = \sqrt{\frac{2}{3}} \cdot \frac{1}{v_\alpha^2 + v_\beta^2} \begin{bmatrix} 1 & 0 \\ -1/2 & \sqrt{3}/2 \\ -1/2 & -\sqrt{3}/2 \end{bmatrix} \cdot \begin{bmatrix} v_\alpha & -v_\beta \\ v_\beta & v_\alpha \end{bmatrix} \cdot \begin{bmatrix} \mathrm{dc}_p \\ 0 \end{bmatrix} \quad (12)$$

$$\begin{bmatrix} i^*_{\mathrm{C},aq\_\mathrm{DC}} \\ i^*_{\mathrm{C},bq\_\mathrm{DC}} \\ i^*_{\mathrm{C},cq\_\mathrm{DC}} \end{bmatrix} = \sqrt{\frac{2}{3}} \cdot \frac{1}{v_\alpha^2 + v_\beta^2} \begin{bmatrix} 1 & 0 \\ -1/2 & \sqrt{3}/2 \\ -1/2 & -\sqrt{3}/2 \end{bmatrix} \cdot \begin{bmatrix} v_\alpha & -v_\beta \\ v_\beta & v_\alpha \end{bmatrix} \cdot \begin{bmatrix} 0 \\ \mathrm{dc}_q \end{bmatrix} \quad (13)$$

The compensating current reference is $i^*_{\mathrm{C},x}$, which consists of $i^*_{\mathrm{C},xq\_\mathrm{DC}}$, $i^*_{\mathrm{C},xp\_\mathrm{DC}}$ and $i_{\mathrm{C},x_{\mathrm{ref}}}$ (obtained from the instantaneous power compensation block). With the hysteresis PWM control (current reference), the loading reactive power and harmonic currents can be compensated through $i_{\mathrm{C},a_{\mathrm{ref}}}$. Moreover, the dc-link voltage control signals with active current $i^*_{\mathrm{C},xq\_\mathrm{DC}}$ and reactive current $i^*_{\mathrm{C},xp\_\mathrm{DC}}$ can effectively achieve the start-up dc-link voltage self-charging function and maintain the dc-link voltage without affecting the dynamic reactive power compensation.

The purpose of adaptive hysteresis band control is to adaptively change the H value to maintain the ATHD (and thus the THD) at its reference value. Referring to the control block in Fig. 6, there are three input variables for the non-linear adaptive hysteresis band controller: the fundamental source current $I_{\mathrm{S},1}$, the target ATHD*, a pre-defined k value. The output variable is the updated hysteresis band H. An initial value is assigned to H when the control system is powered on. The ATHD calculated by (9) is compared with the reference ATHD*. This ATHD error is passed through a transform

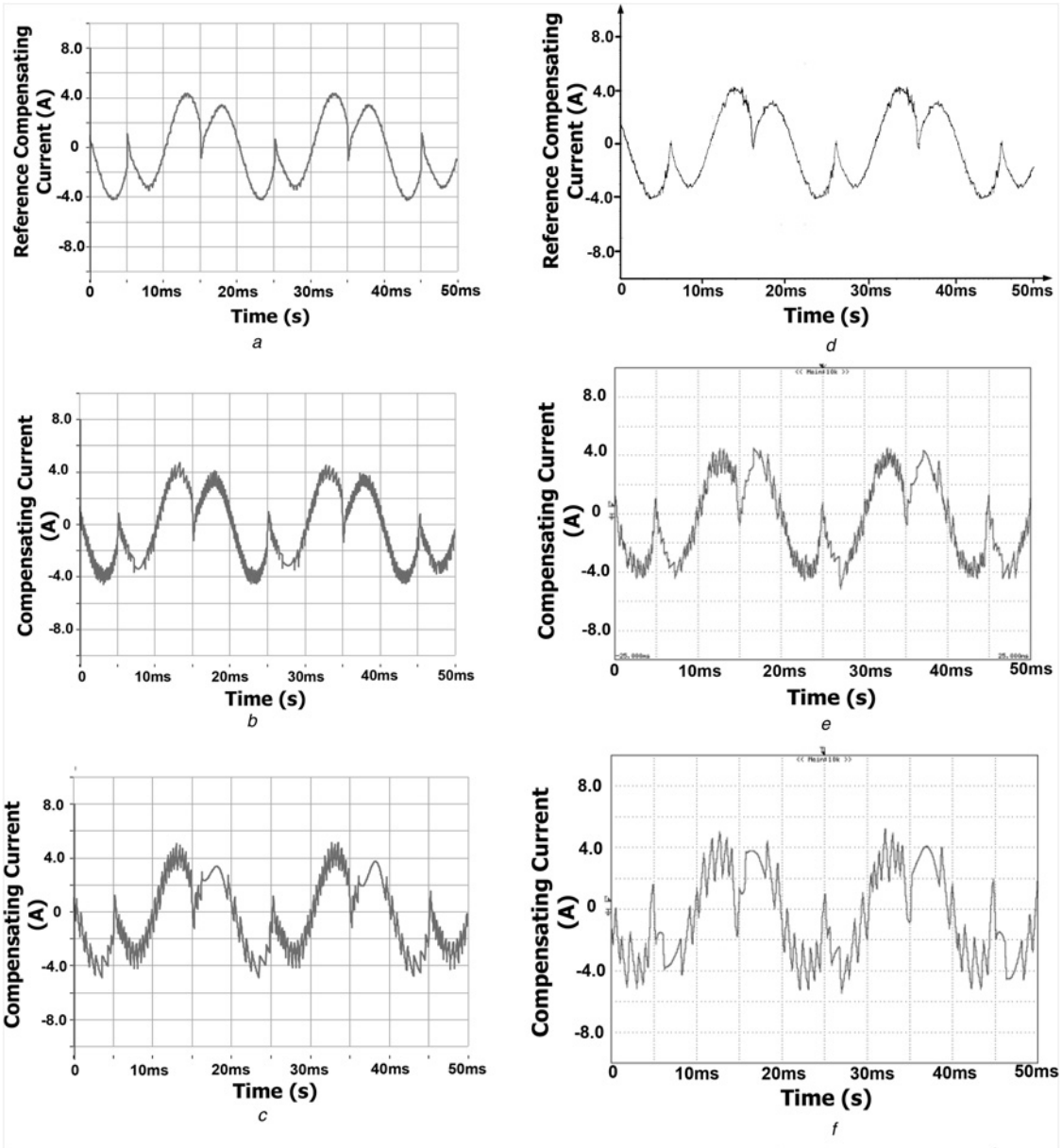

Fig. 7 *Simulated and experimental reference ($i^*_{\mathrm{C},x}$ and $i_{\mathrm{C},x}$, respectively) for compensating first loading case by applying different hysteresis control methods*

a Simulated reference $i^*_{\mathrm{C},x}$
b Simulated $i_{\mathrm{C},x}$ by fixed hysteresis band method [17]
c Simulated $i_{\mathrm{C},x}$ by the proposed method
d Experimental reference $i^*_{\mathrm{C},x}$
e Experimental $i_{\mathrm{C},x}$ by fixed hysteresis band method [17]
f Experimental $i_{\mathrm{C},x}$ by the proposed method

© The Institution of Engineering and Technology 2015

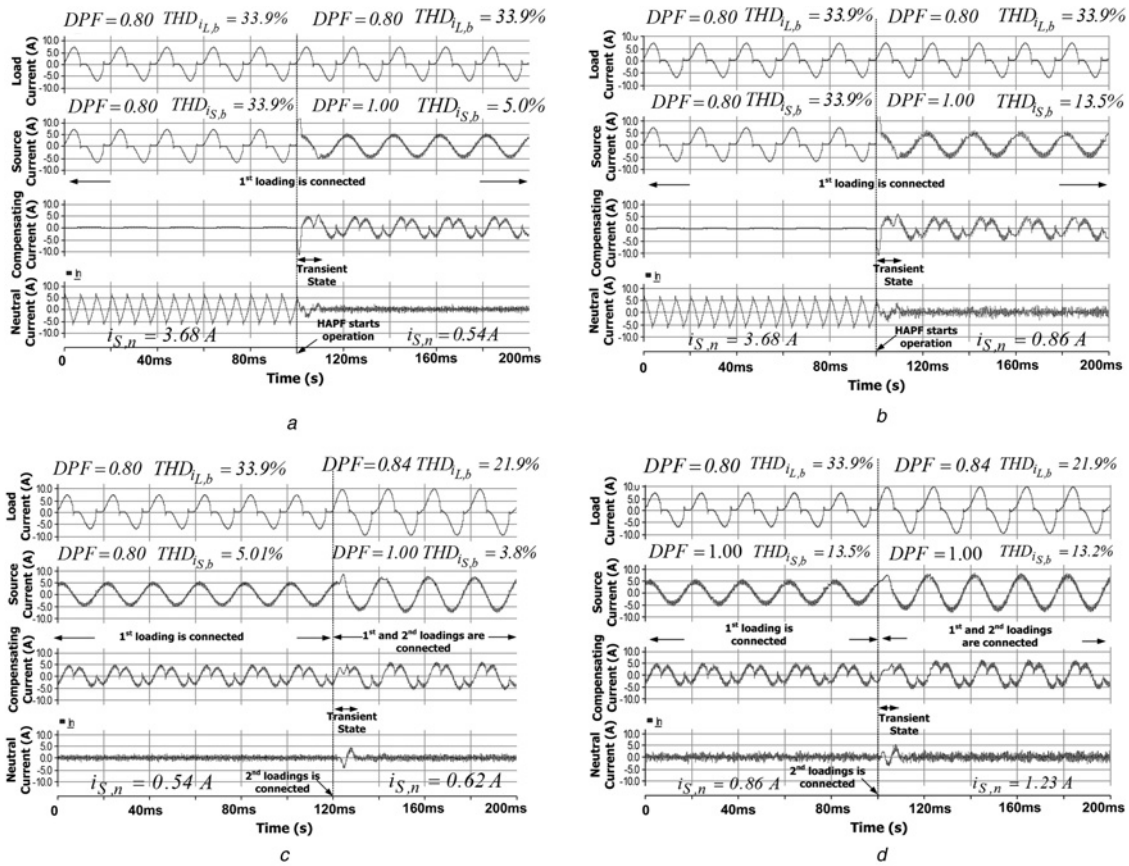

Fig. 8 *Simulation results of dynamic process of phase b load, source and compensating currents and neutral current*

a Waveforms before and after HAPF starts operation by applying fixed hysteresis band controller [17]
b Waveforms before and after starting the HAPF operation by applying the proposed hysteresis band controller
c Waveforms before and after second loading is connected by applying fixed hysteresis band controller [17]
d Waveforms before and after second loading is connected by applying proposed hysteresis band controller

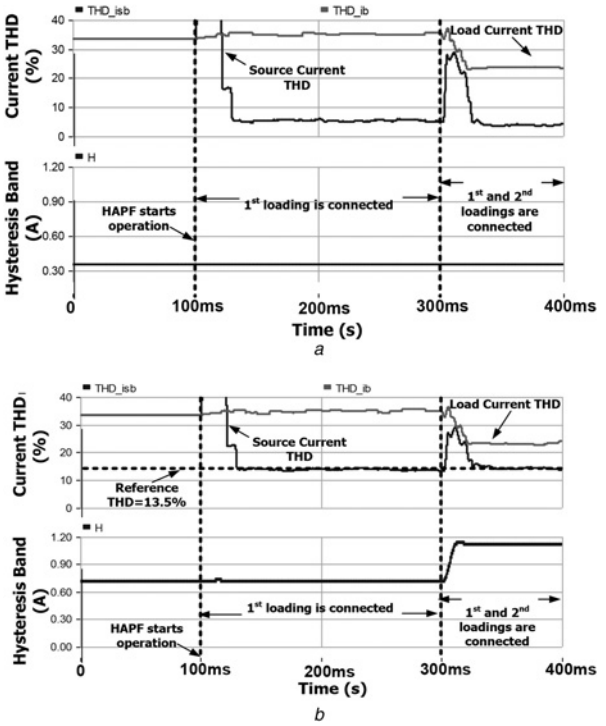

Fig. 9 *Simulated $THD_{iL,b}$, $THD_{is,b}$ and H of phase b during HAPF compensation by applying*

a Conventional fix hysteresis band controller
b Proposed non-linear adaptive hysteresis band controller

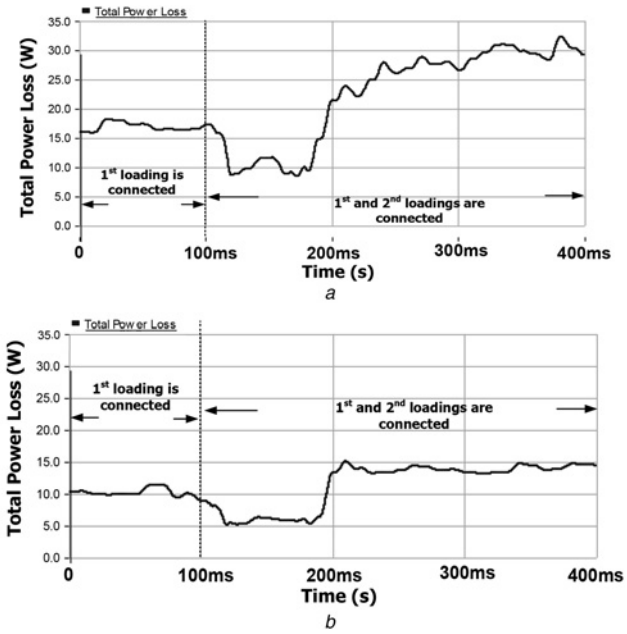

Fig. 10 *Simulated curves of total power loss during the compensation by applying*

a Conventional fix hysteresis band controller
b Proposed non-linear adaptive hysteresis band controller

IET Power Electron., 2015, Vol. 8, Iss. 11, pp. 2156–2167
© The Institution of Engineering and Technology 2015

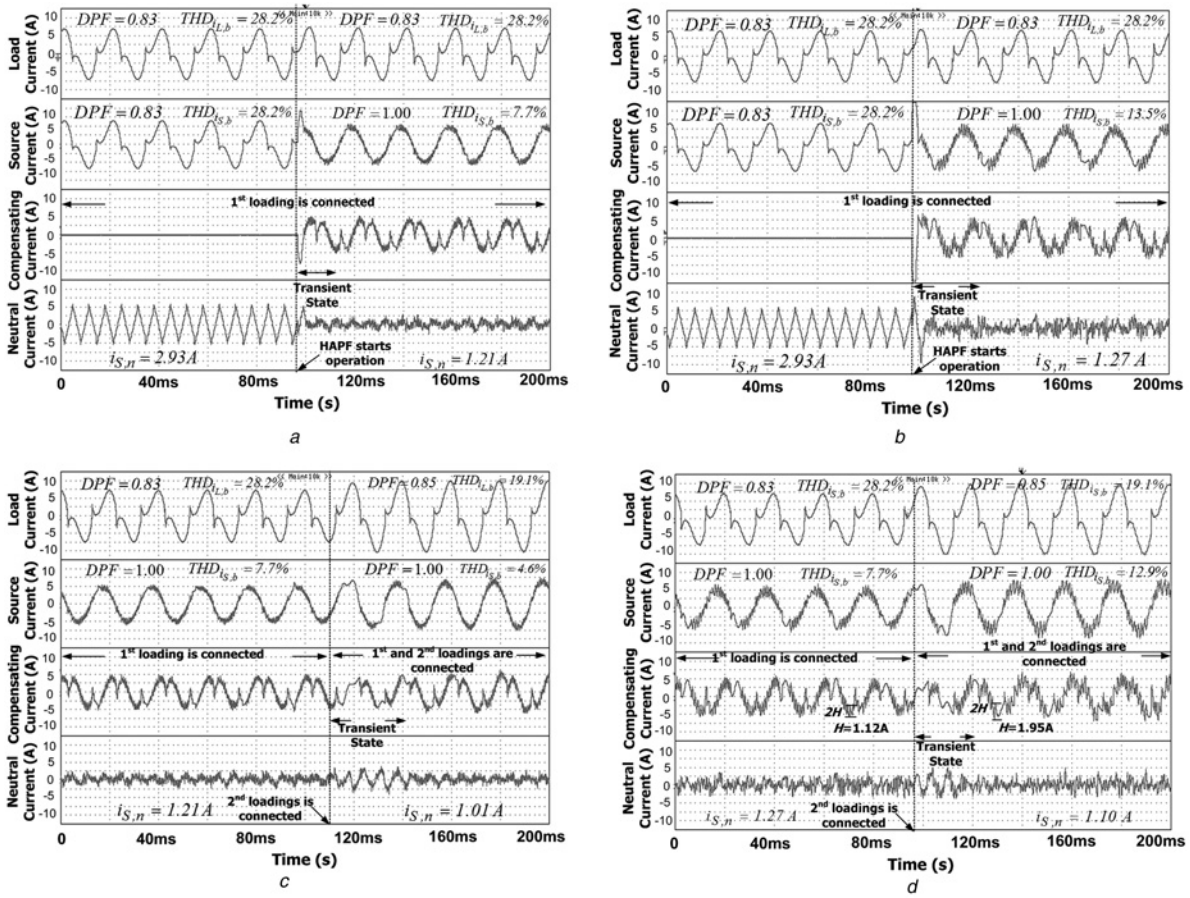

Fig. 11 *Experimental results of dynamic process of phase b load, source and compensating currents and neutral current*

a Waveforms before and after the HAPF starts the operation by applying the fixed hysteresis band controller [17]
b Waveforms before and after the HAPF starts the operation by applying the proposed controller
c Waveforms before and after the second loading is connected by applying the fixed hysteresis band controller [17]
d Waveforms before and after the second loading is connected by applying the proposed controller

function (14) to obtain ΔH. After that, ΔH is added to the H value in previous cycle to adaptively change the H value

$$\Delta H = k_H \cdot (\text{ATHD}^* - \text{ATHD}) \tag{14}$$

The P controller is chosen because it is simpler and faster than a proportional–integral controller. A limiter is applied to avoid the controller's overflow problem. A delay buffer is used to delay H for one sampling period.

In the steady state, the calculated ATHD is approximately equal to ATHD*, so the value of ΔH is close to zero based on (14). That is, the hysteresis band hardly changes. However, in the transient state (when there is a load change), k does not change, whereas $I_{S,1}$ (deduced from (7)) has a stepwise change. Therefore the calculated ATHD in terms of $I_{S,1}$ is different from the reference ATHD*. The value of ΔH is used to adaptively change the value of H. Then, the obtained H is fed back to calculate the ATHD in next cycle. The hysteresis band H in PWM control unit is updated accordingly. This control loop is continuously executed until ATHD gets close enough to its reference.

Under this control, the switching frequency and switching loss can be decreased. As a result, its thermal stress is reduced and the efficiency is increased.

In the following section, the HAPF simulated and experimental results obtained using the proposed non-linear adaptive hysteresis band controller are given in comparison with the fixed hysteresis band linearisation controller proposed in [17].

5 Simulation and experimental results

In this section, the proposed non-linear adaptive hysteresis band PWM controller for HAPFs is investigated using both simulations and experiments. The simulation studies were carried out using power system computer aided design (PSCAD)/electromagnetic transients for direct current (EMTDC). For the experiments, a 110 V and 5 kVA HAPF experimental prototype was designed and constructed in the laboratory. The system parameters, HAPF parameters and testing loads are provided in Table 1. The simulated and experimental results for the proposed non-linear adaptive hysteresis band controlled HAPF are presented in comparison with the results for the fixed hysteresis band linearisation controlled HAPF proposed in [17]. In both the simulations and experiments, the power loss of the HAPF was obtained by measuring the collector–emitter voltage and current of each insulated gate bipolar transistor (IGBT). The total inverter power loss of the HAPF can be found with the following equation [23]

$$P_{\text{loss}} = \sum_{n=0}^{n=6} P_{\text{loss},n} = \sum_{n=0}^{n=6} \frac{1}{t_{\text{f}}} \int_0^{T_{\text{f}}} v_{\text{ce},n}(t) \cdot i_{\text{ce},n}(t)\, \text{d}t \tag{15}$$

where $v_{\text{ce},n}(t)$ and $i_{\text{ce},n}(t)$ are the collector–emitter voltage and current of the IGBT, respectively; t_{f} is the fundamental period and n is the number of IGBTs.

In the following simulations and experiments, the target ATHD* range is set as ATHD* = 13% for the proposed non-linear adaptive hysteresis band control. To keep the HAPF operating in

© The Institution of Engineering and Technology 2015

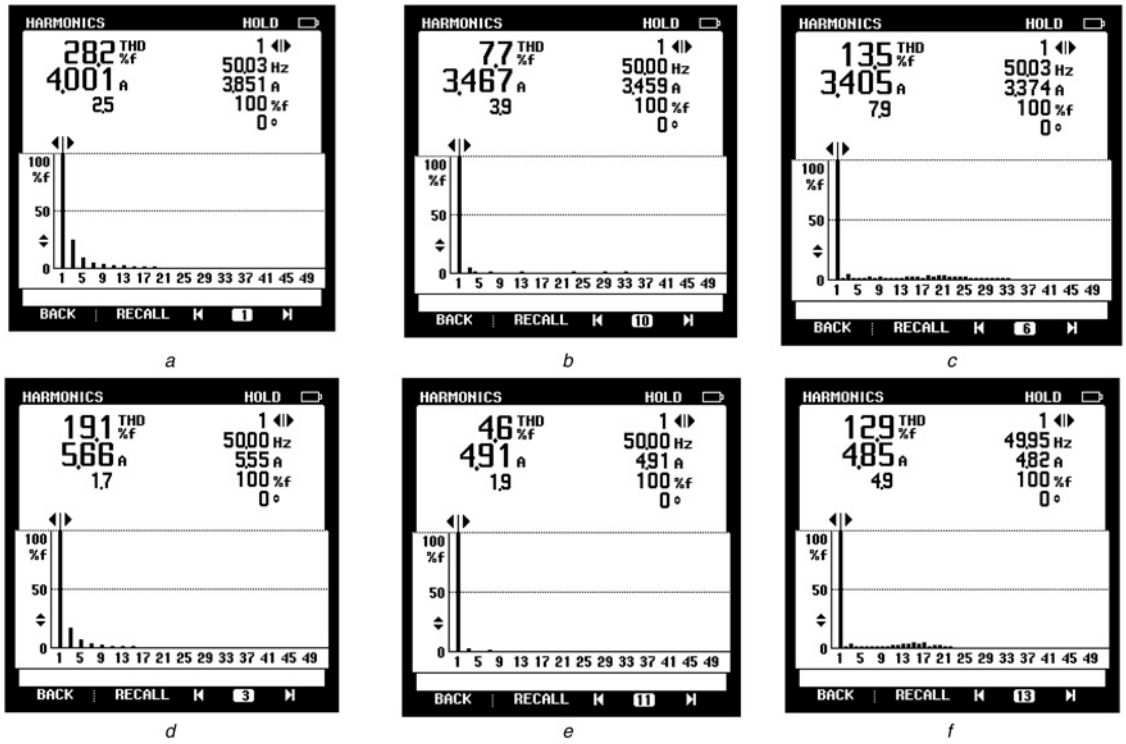

Fig. 12 *Experimental phase b current spectrums during first loading connected case*

a Load current
b Source current after fixed hysteresis band controller compensation [17]
c Source current after the proposed controller compensation during first and second loading connected cases
d Load current
e Source current after fixed hysteresis band controller compensation [17]
f Source current after the proposed controller compensation

the linear region, the chosen H value should satisfy its linear limit H_{linear} [17]. On the basis of [17] and the system parameters in Table 1, H_{linear} can be calculated as $H_{\text{linear}} = 0.4$ A. Therefore by choosing the hysteresis band $H < 0.4$ A, the HAPF will mostly operate in the linear region. As a result, a comparison between the fixed hysteresis band controller [17] and the proposed controller for HAPF can be performed. The simulation and experimental results of the fixed hysteresis band linearisation control method [17] and the proposed non-linear adaptive hysteresis band control method for HAPFs are illustrated in Figs. 7–11, respectively.

Fig. 7 shows the simulation and experimental results of the references $i^*_{C,x}$ and $i_{C,x}$ for the compensating first loading case by applying the fixed hysteresis band linearisation control method [17] and the proposed control method. Figs. 8 and 11 show the simulation and experimental results of the dynamic process of the phase b load, source and compensating currents and the neutral current by applying the fixed hysteresis band control method [17] and the proposed control method during the load transient. Fig. 9 illustrates the dynamic waveforms of the load current THD, source current THD and H by applying the fix hysteresis band controller and the proposed adaptive non-linear hysteresis band controller to HAPF. Fig. 10 shows the curves of the total power loss during the compensation from applying the fixed hysteresis band controller [17] and the proposed adaptive non-linear hysteresis band controller. Fig. 12 provides the experimental load and source current spectrums after applying the fixed hysteresis band controller [17] and proposed adaptive non-linear controller compensation. Tables 2 and 3 summarise the simulation and experimental results, respectively.

Under the fixed hysteresis band control (Figs. 7*b* and *e*), the compensating current $i_{C,x}$ falls mostly in the linear region, which can be verified by the simulated and experimental values of $(t_{\text{quasi}} + t_{\text{non-linear}})/t_{\text{f}} < 7\%$ given in Tables 2 and 3. As shown by Figs. 8, 11 and 12 and Tables 2 and 3, the simulated and experimental system displacement power factors (DPFs) are close to unity during both the first and second loading connected cases. As seen in Figs. 9*a* and 12, the simulated and experimental THDs are lower than 10% compared with the simulated THD value of 33.9% (worst phase) and the experimental THD value of 28.2% (worst phase) before compensation. After connecting the second loading, the simulated and experimental system DPFs can still be kept at unity with loading DPFs of 0.84 and 0.85, respectively. Moreover, the simulated and experimental THDs are lower than 5% compared with the simulated THD value of 21.9% (worst phase) and the experimental THD value of 19.1% (worst phase) before compensation. In addition, the simulated and experimental system neutral current $i_{S,n}$ is significantly reduced after compensation.

After the fixed hysteresis band controlled HAPF [17] operates, the simulated and experimental average switching frequency (f_{sw}) and inverter power loss ($P_{\text{VSI\_loss}}$) of the HAPF are $f_{\text{sw}} = 4.01$ kHz and $P_{\text{VSI\_loss}} = 16.4$ W (simulation results, Fig. 10*a*) and $f_{\text{sw}} = 2.86$ kHz and $P_{\text{VSI\_loss}} = 21.3$ W (experimental results, Table 1) for the first loading case and $f_{\text{sw}} = 4.96$ kHz and $P_{\text{VSI\_loss}} = 30.2$ W (simulation results, Fig. 10*a*) and $f_{\text{sw}} = 2.51$ kHz and $P_{\text{VSI\_loss}} = 36.3$ W (experimental results, Table 1) for the first and second loading cases.

Figs. 7*c* and *f* show that using the proposed non-linear adaptive hysteresis band control method, the possibility of the compensating current $i_{C,x}$ falling in the quasi-linear and non-linear regions is higher than that resulting from the fixed hysteresis band method; the simulated and experimental values of $(t_{\text{quasi}} + t_{\text{non-linear}})/t_{\text{f}} > 14\%$ are shown in Tables 2 and 3. From Fig. 11 and Tables 2 and 3, the simulated and experimental system DPF is compensated to unity during both loading cases. Figs. 9*b* and11*d* (the curve of $i_{c,x}$) and Fig. 12 show that the value of H adaptively changes to maintain the THD value around its reference value (satisfying the IEEE Standard [20]) when the loading varies. Moreover, the simulated and experimental system neutral current $i_{S,n}$ is significantly reduced after compensation.

Following the HAPF compensation, the simulated and experimental average switching frequency (f_{sw}) and inverter power loss ($P_{\text{VSI\_loss}}$) of the HAPF are $f_{\text{sw}} = 2.12$ kHz and $P_{\text{VSI\_loss}} = 9.8$

© The Institution of Engineering and Technology 2015

Table 2 Simulated results for fixed hysteresis band linearisation controller [17] and the proposed non-linear adaptive hysteresis band controller before and after compensation

		First loading			First and second loadings		
		Before compensation	Linearisation method [17]	Proposed method	Before compensation	Linearisation method [17]	Proposed method
$i_{S,x}$, A	A	3.95	3.22	3.21	5.88	4.86	4.87
	B	3.95	3.22	3.21	5.88	4.86	4.87
	C	3.95	3.22	3.21	5.88	4.86	4.87
$i_{S,n}$, A	N	3.68	0.54	0.86	3.64	0.62	1.23
DPF, %	A	0.8	1	1	0.84	1	1
	B	0.8	1	1	0.84	1	1
	C	0.8	1	1	0.84	1	1
$THD_{is,x}$, %	A	33.9	5	13.5	21.9	3.8	13.2
	B	33.9	5	13.5	21.9	3.8	13.2
	C	33.9	5	13.5	21.9	3.8	13.2
$(t_{non\text{-}linear} + t_{quasi})/t_f$, %		—	4.1	14.1	—	5.5	15.1
average f_{sw}, Hz		—	4.01 k	2.12 k	—	4.96 k	1.93 k
P_{VSI_loss}, W		—	16.4	9.8 0 (↓40.2%)	—	30.2	15.8 (↓47.6%)

Table 3 Experimental results for fixed hysteresis band linearisation controller [17] and proposed non-linear adaptive hysteresis band controller before and after compensations

		First loading			First and second loadings		
		Before compensation	Linearisation method [17]	Proposed method	Before compensation	Linearisation method [17]	Proposed method
$i_{S,x}$, A	A	4	3.5	3.44	5.65	4.96	4.99
	B	4	3.47	3.4	5.66	4.91	4.85
	C	3.94	3.47	3.55	5.54	4.88	4.85
$i_{S,n}$, A	N	2.93	1.21	1.27	2.87	1.01	1.1
DPF, %	A	0.83	1	1	0.85	1	1
	B	0.83	1	1	0.85	1	1
	C	0.83	1	1	0.85	1	1
$THD_{is,x}$, %	A	27.8	9.3	15	19	5	12.6
	B	28.2	7.7	13.5	19.1	4.6	12.9
	C	27.4	7.7	12.7	18.8	5	12.1
$(t_{non\text{-}linear} + t_{quasi})/t_f$, %		—	6.2	20.1	—	4.7	19.2
average f_{sw}, Hz		—	2.86 k	1.21 k	—	2.51 k	0.95 k
P_{VSI_loss}, W		—	21.3	11.6 (↓45.5%)	—	36.3	18.6 (↓48.8%)

W (simulation results, Fig. 10*b*) and $f_{sw} = 1.21$ kHz and $P_{VSI\_loss} = 11.6$ W (experimental results, Table 2) for the first loading case and $f_{sw} = 1.93$ kHz and $P_{VSI\_loss} = 15.8$ W (simulation results, Fig. 10*b*) and $f_{sw} = 0.95$ kHz and $P_{VSI\_loss} = 18.6$ W (experimental results, Table 2) for the first and second loading cases.

By comparing the simulated and experimental results between the fixed hysteresis band linearisation controlled HAPF and the proposed non-linear adaptive hysteresis band controlled HAPF, Fig. 7 and Tables 2 and 3 show that the average switching frequencies of the proposed method are lower than those of the linearisation method. Moreover, the total simulated and experimental inverter power loss of the HAPF can be reduced by more than 40% when the proposed method is applied. Figs. 7–12 and Tables 2 and 3 verify the deduced ATHD and the effectiveness of the proposed non-linear adaptive hysteresis band PWM controller for HAPFs in reducing inverter power loss and maintaining the THD at the desired value.

6 Conclusion

In this paper, a non-linear adaptive hysteresis band PWM controller for HAPFs is proposed to reduce the switching loss and maintain the source current THD to within user requirements (satisfying IEEE Standards). Owing to the circuit configuration of the HAPF, the non-linear characteristics of its compensating current are discussed in relation to the linear, quasi-linear and non-linear operating regions. By comparing the proposed method with the previous fixed hysteresis band controller [17], this paper proposes that the compensating current can be controlled to operate in the non-linear or quasi-linear regions, rather than always staying in the linear region. To simplify the calculation, an ATHD index is proposed and deduced to speed up the HAPF system respond time. Using the deduced direct relationship between the hysteresis band H and ATHD, a non-linear adaptive hysteresis band PWM controller for HAPFs is proposed. Finally, simulated and experimental results for the proposed non-linear adaptive hysteresis band controlled HAPF are presented, which verify the deduced ATHD and the effectiveness of the proposed adaptive controller for HAPF to reduce the switching loss and maintain an acceptable source current THD. On the basis of the experimental results, the proposed method reduces the loss by more than 45%.

7 Acknowledgement

This work is supported by the Macao Science and Technology Development Fund (FDCT) (FDCT 109/2013/A3) and the Research Committee of University of Macau (MRG012/WMC/2015/FST, MYRG137 (Y1-L4)-FST12-WMC).

8 References

1 Srianthumrong, S., Akagi, H.: 'A medium-voltage transformerless ac/dc power conversion system consisting of a diode rectifier and a shunt hybrid filter', *IEEE Trans. Ind. Appl.*, 2003, **39**, (3), pp. 874–882
2 Rahmani, S., Hamadi, A., Mendalek, N., Al-Haddad, K.: 'A new control technique for three-phase shunt hybrid power filter', *IEEE Trans. Ind. Electron.*, 2009, **56**, (8), pp. 2904–2915
3 Salmeron, P., Litran, S.P.: 'A control strategy for hybrid power filter to compensate four-wires three-phase systems', *IEEE Trans. Power Electron.*, 2010, **25**, (7), pp. 1923–1931
4 Corasaniti, V.F., Barbieri, M.B., Arnera, P.L., Valla, M.I.: 'Hybrid active filter for reactive and harmonics compensation in a distribution network', *IEEE Trans. Ind. Electron.*, 2009, **56**, (3), pp. 670–677

© The Institution of Engineering and Technology 2015

5 Jiang, W., Li, W., Wu, Z., She, Y., Tao, Z.: 'Space-vector pulse-width modulation algorithm for multilevel voltage source inverters based on matrix transformation and including operation in the over-modulation region', *IET Power Electron.*, 2014, **7**, (12), pp. 2925–2933
6 Mao, X., Ayyanar, R., Krishnamurthy, H.K.: 'Optimal variable switching frequency scheme for reducing switching loss in single-phase inverters based on time-domain ripple analysis', *IEEE Trans. Power Electron.*, 2009, **24**, (4), pp. 991–1001
7 Jiang, D., Wang, F.: 'Variable switching frequency PWM for three-phase converters based on current ripple prediction', *IEEE Trans. Power Electron.*, 2013, **28**, (11), pp. 4951–4961
8 Zhang, D., Wang, F., El-Barbari, S.: 'Improved asymmetric space vector modulation for voltage source converters with low carrier ratio', *IEEE Trans. Power Electron.*, 2012, **27**, (3), pp. 1130–1140
9 Wei, L., Lukaszewski, R.A.: 'Pulse width modulation (PWM) rectifier with variable switching frequency'. U.S. patent 7 190 143 132, March 2007
10 Angélico, B.A., Campanhol, L.B., da Silva, S.A.O.: 'Proportional–integral/proportional–integral-derivative tuning procedure of a single-phase shunt active power filter using bode diagram', *IET Power Electron.*, 2014, **7**, (10), pp. 2647–2659
11 Hamad, M.S., Masoud, M.I., Williams, B.W., Finney, S.: 'Medium voltage 12-pulse converter: ac side compensation using a shunt active power filter in a novel front end transformer configuration', *IET Power Electron.*, 2012, **5**, (8), pp. 1315–1323
12 Zobaa, A.F.: 'Optimal multiobjective design of hybrid active power filters considering a distorted environment', *IEEE Trans. Ind. Electron.*, 2014, **61**, (1), pp. 107–114
13 Wu, J.C., Jou, H.L., Hsaio, H.H., Xiao, S.T.: 'A new hybrid power conditioner for suppressing harmonics and neutral-line current in three-phase four-wire distribution power systems', *IEEE Trans. Power Deliv.*, 2014, **29**, (4), pp. 1525–1532
14 Lam, C.S., Choi, W.H., Wong, M.C., Han, Y.D.: 'Adaptive DC-link voltage-controlled hybrid active power filters for reactive power compensation', *IEEE Trans. Power Electron.*, 2012, **27**, (4), pp. 1758–1772
15 Khadem, S.K., Basu, M., Conlon, M.F.: 'Harmonic power compensation capacity of shunt active power filter and its relationship with design parameters', *IET Power Electron.*, 2014, **7**, (2), pp. 418–430
16 Chauhan, S.K., Shah, M.C., Tiwari, R.R., Tekwani, P.N.: 'Analysis, design and digital implementation of a shunt active power filter with different schemes of reference current generation', *IET Power Electron.*, 2014, **7**, (3), pp. 627–639
17 Lam, C.S., Wong, M.C., Han, Y.D.: 'Hysteresis current control of hybrid active power filters', *IET Power Electron.*, 2012, **5**, (7), pp. 1175–1187
18 Lam, C.S., Wong, M.C., Choi, W.H., Cui, X.X., Mei, H.M., Liu, J.Z.: 'Design and performance of an adaptive low dc voltage controlled LC-hybrid active power filter with a neutral inductor in three-phase four-wire power systems', *IEE Trans. Ind. Electron.*, 2014, **61**, (6), pp. 2635–2647
19 Choi, W.H., Lam, C.S., Wong, M.C., Han, Y.D.: 'Analysis of dc-link voltage controls in three-phase four-wire hybrid active power filters', *IEEE Trans. Power Electron.*, 2013, **28**, (5), pp. 2180–2191
20 IEEE Standard 519-2014: 'IEEE recommended practices and requirements for harmonic control in electrical power systems', 2014
21 Shmilovitz, D.: 'On the definition of total harmonic distortion and its effect on measurement interpretation', *IEEE Trans. Power Deliv.*, 2005, **20**, (1), pp. 526–528
22 Peng, F.Z., Lai, J.S.: 'Generalized instantaneous reactive power theory for three-phase power systems', *IEEE Trans. Instrum. Meas.*, 1996, **45**, (1), pp. 293–297
23 Xiao, C., Chen, G., Odendaal, W.G.: 'Overview of power loss measurement techniques in power electronics systems', *IEEE Trans. Ind. Appl.*, 2007, **43**, (3), pp. 657–664

9 Appendix

The deductions of (4) are discussed separately in two regions: the linear region (see Fig. 13) and non-linear region (see Fig. 14).

In the linear region, the current error in a fundamental period is equal to the RMS value of the *n*th individual irregular triangular waveform. To calculate the RMS value of the triangular-like current error signal, a mathematical model can be established as follows

$$i_{\mathrm{e}} = \begin{cases} k_1(t-t_0)-H, & t_0 < t < t_1 \\ k_2(t-t_1)-H, & t_1 < t < t_2 \\ \cdots & \cdots \\ k_n(t-t_{n-1})-H, & t_{n-1} < t < t_{\mathrm{f}} \end{cases} \tag{16}$$

The current error can be calculated by substituting (16) into the current error (4), yielding (see (17))

From (17), it can be seen that $k = \sqrt{3}$ when the entire current period is in the linear region (see Fig. 13).

In the non-linear region, the current error in a fundamental period is equal to the RMS value of the *n*th individual sinusoidal-like waveform. To calculate the current error signal, a mathematical model can be established as follows

$$i_{\mathrm{e}} = \begin{cases} A_1 \cdot \sin(\omega_0 t + \phi_1), & t_0 < t < t_1 \\ A_2 \cdot \sin(\omega_0 t + \phi_2), & t_1 < t < t_2 \\ \cdots & \cdots \\ A_n \cdot \sin(\omega_0 t + \phi_n), & t_{n-1} < t < t_{\mathrm{f}} \end{cases} \tag{18}$$

The current error can be calculated by substituting (18) into the current error (4), yielding (see (19))

where t_{f} is the fundamental period and $\omega_0 = \left(1/\sqrt{L_{\mathrm{C}} \cdot C_{\mathrm{C}}}\right)$. For the worst case, each sinusoidal-like waveform can just touch the hysteresis band H and $k = \sqrt{2}$.

$$\begin{aligned} I_{\mathrm{e}} &= \sqrt{\frac{1}{t_{\mathrm{f}}}\left(\int_{t_0}^{t_1} i_{\mathrm{e}}^2\,\mathrm{d}t + \int_{t_1}^{t_2} i_{\mathrm{e}}^2\,\mathrm{d}t + \cdots + \int_{t_{n-1}}^{T_{\mathrm{f}}} i_{\mathrm{e}}^2\,\mathrm{d}t\right)} \\ &= \sqrt{\frac{1}{t_{\mathrm{f}}}\left(\int_{t_0}^{t_1} \left[k_1(t-t_1)-H\right]^2\,\mathrm{d}t + \int_{t_1}^{t_2} \left[k_2(t-t_1)-H\right]^2\,\mathrm{d}t + \cdots + \int_{t_{n-1}}^{t_{\mathrm{f}}} \left[k_{n2}(t-t_n)-H\right]^2\,\mathrm{d}t\right)} \\ &= \sqrt{\frac{1}{t_{\mathrm{f}}}\left(\frac{H^2\cdot(t_1-t_0)}{3} + \frac{H^2\cdot(t_2-t_1)}{3} + \cdots + \frac{H^2\cdot(t_{\mathrm{f}}-t_{n-1})}{3}\right)} \\ &= \frac{H}{\sqrt{3}} \end{aligned} \tag{17}$$

$$\begin{aligned} I_{\mathrm{e}} &= \sqrt{\frac{1}{t_{\mathrm{f}}}\left(\int_{t_0}^{t_1} i_{\mathrm{e}}^2\,\mathrm{d}t + \int_{t_1}^{t_2} i_{\mathrm{e}}^2\,\mathrm{d}t + \cdots + \int_{t_{n-1}}^{t_{\mathrm{f}}} i_{\mathrm{e}}^2\,\mathrm{d}t\right)} \\ &= \sqrt{\frac{1}{t_{\mathrm{f}}}\left(\int_{t_0}^{t_1} A_1^2\sin^2(\omega_0 t+\phi_1)\,\mathrm{d}t + \int_{t_1}^{t_2} A_2^2\sin^2(\omega_0 t+\phi_2)\,\mathrm{d}t + \cdots + \int_{t_{n-1}}^{t_{\mathrm{f}}} A_n^2\sin^2(\omega_0 t+\phi_n)\,\mathrm{d}t\right)} \\ &\simeq \frac{H}{\sqrt{2}}\sqrt{\frac{1}{t_{\mathrm{f}}}\cdot\left[(t_1-t_0)+(t_2-t_1)+\cdots+(t_{\mathrm{f}}-t_{n-1})\right]} \\ &\simeq \frac{H}{\sqrt{2}} \end{aligned} \tag{19}$$

© The Institution of Engineering and Technology 2015

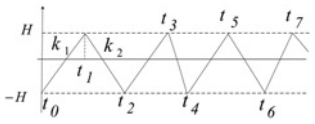

Fig. 13 *Error current signal of hysteresis controller in linear region*

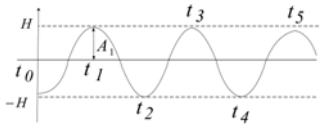

Fig. 14 *Error current signal of hysteresis controller in non-linear region*

© The Institution of Engineering and Technology 2015